Transactions of The Indian Institute of Metals
Vol. 62, Issues 4-5, August-October 2009, pp. 455-460

Interferometric method for the analysis of dendrite growth and shape in 3D extended patterns in transparent alloys

N. Bergeon[1,2], C. Weiss[1,2], N. Mangelinck-Noël[1,2] , B. Billia[1,2]

[1] Aix Marseille Université and [2] CNRS, IM2NP, Campus Saint-Jérôme, Case 142, 13397 Marseille Cedex 20, France

Email: nathalie.bergeon@im2np.fr

Received 23 July 2009
Revised 8 October 2009
Accepted 12 October 2009
Online at www.springerlink.com

Keywords:
directional solidification; dendrites; interferometry; transparent alloys

Abstract

In the frame of the DECLIC project of the French Space Agency (CNES), a specific device dedicated to the in situ and real time observation of directional solidification of transparent systems in 3D configuration has been developed. A method based on interferometric analysis is presented to quantitatively characterize the shape and growth of dendrites so that measurements of critical parameters such as tip radius and growth rate of individual dendrites belonging to extended patterns are enabled. First results obtained on a succinonitrile - 0.1 wt% camphor alloy are analysed. The accuracy of measurements and quality of the shape reconstruction are discussed through the comparison of the dendrite contours obtained with different modellings of the dendritic shape (parabolic, parabolic corrected by a 4^{th} order term, power-law).

1. Introduction

The formation of solidification microstructure is very important in the design and processing of new materials [1]. The interface patterns formed by solidification largely govern mechanical and physical properties of materials, so that materials and processing conditions can be designed to obtain specific patterns which give optimum properties and better reliability of the finished product. Dendritic patterns are found in most casting and welding microstructures. An improved understanding of the solidification microstructure formation, and especially of the dendritic one, will lead to a better control of material properties.

Among the parameters that are usually measured to characterize dendrites, the tip velocity V_{tip} and the tip radius R are of particular interest as experiments revealed that they are uniquely determined by the supercooling or the supersaturation in case of free growth [2,3]. For directional solidification, a unique tip radius is obtained for steady-state growth at given velocity and concentration [4]. This situation is consistent with the statements of the most recent theories on dendritic growth. The earliest theory that attempted to analyse dendritic growth leads to the well-known Ivantsov solution [5] that describes the dendrite tip as a rotational paraboloid for which $V_{tip}R^2$ is uniquely determined by the supercooling. This theory does not explain the sharp selection of tip radius experimentally observed since a continuum of solution exists for R. However, some of Ivantsov hypotheses had to be corrected as anisotropy, surface tension and kinetic effects were neglected in his calculations. A linear stability analysis taking into account the surface tension has been developed by Langer and Müller-Krumbhaar [6]; it appeared that only a range of radius values among the Ivantsov solutions is stable. The unique operating point is quite arbitrary chosen as the marginally stable dendrite tip radius, so that $V_{tip}R^2$ is uniquely determined and only depends on the material. Even if experimental results are consistent with this marginal stability theory, one of its major drawback is to neglect anisotropy since solely isotropic capillarity is included. Further development led to the so-called microscopic solvability theory [7] that predicts the existence of a discrete set of solutions with only the fastest one stable against tip-splitting when the anisotropy of surface tension is included. The interesting point is that the relationship between V_{tip} and R coming from this theory is exactly similar to the one obtained from marginal stability, except that the characteristic constant σ^* of this relation becomes dependent on the system anisotropy.

This brief review emphasizes the tremendous efforts that have been devoted during the past decades to experimentally characterize dendrite tips. However, this characterization is not evident as post-mortem determination of tip parameters is extremely difficult to perform. In situ determinations are more reliable so that such studies have been conducted on some special organic systems that are analogous to metallic systems in term of solidification behavior but have the great interest of being transparent to visible light. For directional solidification, studies have been carried out with those materials in a configuration where the sample is constrained between two narrowly-spaced plates [4,8,9]. Although very interesting and fruitful, this quasi-2D configuration is neither representative of materials processing nor capable of producing extended 3D solidification patterns [10].

In the frame of the DECLIC project of the French Space Agency (CNES), a specific device (called DECLIC-DSI) dedicated to the directional solidification of transparent systems in 3D configuration has been developed that enables the continuous and in situ observation of the solid-liquid interface. We here present a method and the first results of

accurate characterization of the dendrite tips performed with this instrument through interferometric measurements.

2. Materials and methods

2.1. Experimental set-up

The present study was conducted in the laboratory model of the DECLIC-DSI. Upward solidification is achieved by pulling the crucible containing the alloy (Succinonitrile (SCN) – 0.1 wt% Camphor) down into the cold zone of a Bridgman furnace at a rate V_P ranging from 0.1 to 20 μm/s. The thermal field is characterized by the temperature gradient G established between a cold and a hot zones. A more detailed description of this device has been given previously [11, 12]. The crucible is a cylindrical glass tube with an inner diameter of ten millimetres and a length that allows about ten centimetres of solidification, thus enabling the study of the whole development of extended 3D patterns from the initial stage to the steady state. The design of the system makes possible the interface observation from the top as well as from the side to get its macroscopic shape.

It is worth noting that a single crystal with one <100> direction parallel to the crucible axis, i.e. parallel to the observation axis, is first grown and kept as solid seed for further growths. This orientation is required for a good observation of dendrites. The technique developed to grow such single crystals is described in Weiss et al. [13].

2.2. Principles of the interferometric analysis

The DECLIC-DSI is equipped with an interferometer settled on the axial direction of the crucible, using a polarised He-Ne laser (wavelength λ=632.8 nm). The analysis of interferometric images is used to determine the interface shape and its motion. Interference fringes appear at the recombination of the laser beam passing through the crucible with a reference beam passing outside. The fringes result from the difference of optical paths between those two beams. Passing from one fringe to the following one corresponds to a variation of the object optical path which equals λ. This observation mode provides patterns of fringes that can be considered as interface level curves.

During the experiment, the main variations of optical paths are attributed to variations of the lengths of different phases (solid / liquid). Space variation is obtained by comparing the optical paths of parallel rays crossing the interface at different places but at the same time t; corresponding interferometric fringes are related to the interface shape. Time variation is obtained by comparing the optical paths of one ray at different times; the observed sliding of fringes is due to the motion of the interface. It is worth noting that, in the following developments, the effects of concentration variations on refractive indices are neglected considering the fact that alloys of very low solute concentrations are used; refractive indices are thus considered solely temperature-dependent.

- ***Space variation***

As illustrated in figure 1a, the optical paths (OP) of the two rays at a time t differ only close to the interface, on the thickness L, which is solid for ray 1 and liquid for ray 2. The temperature field surrounding the interface is considered homogeneous along the interface. If 1 and 2 correspond to two side by side fringes, then:

$$OP_1 - OP_2 = L(n_{\phi S} - n_{\phi L}) = \lambda \Rightarrow \lambda = L\Delta n_\phi \quad (1)$$

with : L, difference in solid length between rays 1 and 2

λ, laser wavelength

$n_{\phi S}$, refractive index of solid at the interface temperature

$n_{\phi L}$, refractive index of liquid at the interface temperature

$\Delta n_\phi = n_{\phi S} - n_{\phi L}$, difference of refractive indices between solid and liquid at the interface

- ***Time variation***

In case of stationary growth, the interface position is fixed in the furnace frame (the interface rate V is equal to the pulling rate V_P). As represented in figure 1b, during a time Δt, the length of solid increases of $V_P\Delta t$ and the length of liquid respectively decreases of the same quantity. The optical path of a ray taken at times t and t+Δt is consequently modified:

$$OP(t+\Delta t) - OP(t) = V_P\Delta t(n_s(T_{CZ}) - n_L(T_{HZ}))$$

with : $n_S(T_{CZ})$, efractive index of solid at the temperature of the cold zone T_{CZ}

$n_L(T_{HZ})$, refractive index of liquid at the temperature of the hot zone T_{HZ}

If Δt corresponds to the crossing of 1 fringe, then :

$$\lambda = \Delta t V_P \Delta n_{SL} \quad (2)$$

with : $\Delta n_{SL} = n_S(T_{CZ}) - n_L(T_{HZ})$, difference of refractive indices between cold solid and hot liquid

- ***Refractive indices***

It clearly appears from expressions (1) and (2) that the knowledge of refractive indices in both solid and liquid phases, and of their variations with temperature and solute concentration, is critical to extract quantitative data from interferometric images. Several measurements have been performed to determine the variation of the refractive index of pure SCN in liquid phase as a function of temperature, but they are usually not completed by similar data in solid state ([14], unpublished data from Liu & Trivedi or other unpublished data from Zeiss). The differences of optical indices required for our analysis are calculated on the basis of the only complete characterization of the SCN refractive indices as a function of T, for both phases, that has been done by MacFarlane et al. [15]. Using their data:

$$\Delta n_\phi = 0.0190$$

$$\Delta n_{SL} = 0.0340$$

2.3 Interferometric analysis applied to dendrites

An example of interferometric image of a few dendrites is given in Fig. 2a; these dendrites belong to the pattern

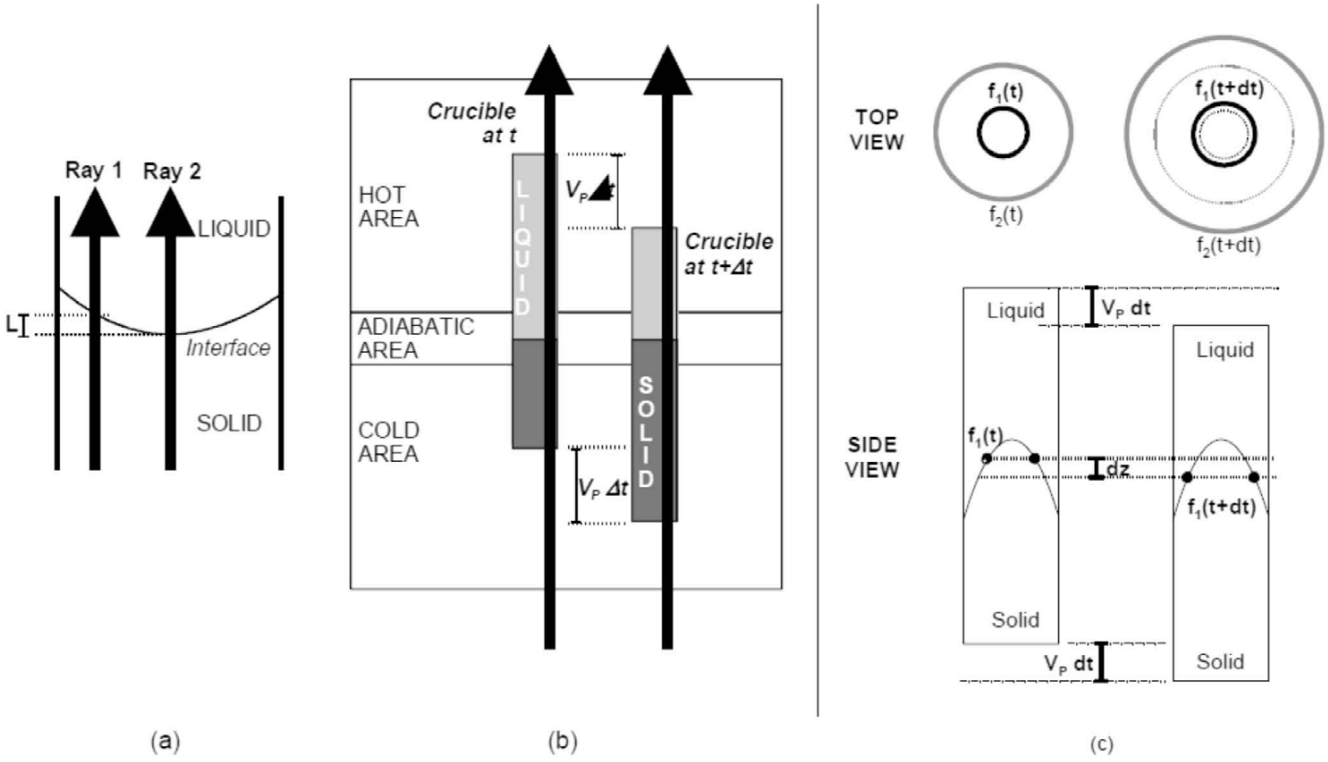

Fig. 1 : Interferometry analysis of stationary growth
a) Spatial analysis: comparison of optical paths of two rays at the same time
b) Time analysis: evolution of the optical path of one ray between t and t+Δt
c) Principle of dendrite profile analysis. The top-view is a schematic representation of real interferometric images. Side view enables to visualize the variation of composition of the optical path of fringe 1 between t and t+dt

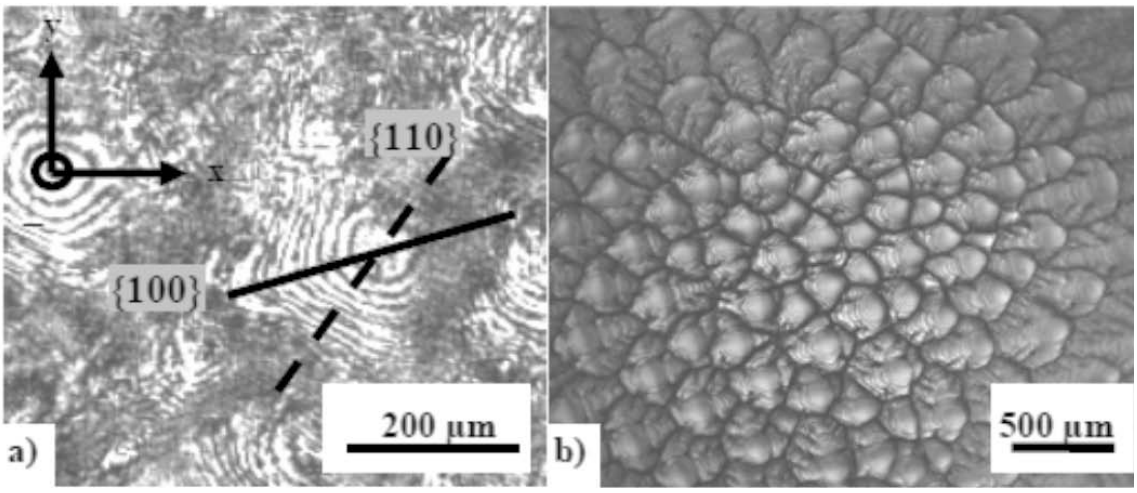

Fig. 2 : a) Top-view direct observation of the whole dendritic pattern.
b) Enlarged view of the corresponding interferogram
Succinonitrile –0.1 wt% camphor; V_p = 20 µm/s; G = 17 K/cm

presented in Fig. 2b (direct top-view observation). On each image, 4 to 5 fringes are neatly seen on a dendrite tip to rebuild its shape. A software developed in collaboration with H. Singer of ETHZ gives us the locus of each fringe in a coordinate system (x,y) centred on the dendrite tip. Relation (1) can be applied with $\Delta n_\phi = 0.0190$ so that we can attribute a height to each fringe, setting the point z = 0 on the centre of the tip and taking that 2 neighbouring fringes correspond to a height difference of 33.3 µm. The dendrite profile is therefore described by 4 or 5 points, which is not sufficient to precisely rebuild the tip shape. This is the reason why this spatial analysis is combined with temporal analysis by using several successive images of the same dendrite.

The principle is described in Fig. 1c. The top view corresponds to a schematic representation of 2 fringes f_1 and f_2 located on a dendrite tip, at 2 different times. At t, these 2 fringes give 2 points on the dendrite profile as described previously. Let us consider for example the motion of the fringe noted f_1 between t and t+dt. A fringe corresponds to a precise value of the optical path so that the optical paths of f_1 at both t and t+dt are the same. The side view of Fig. 1c points out the evolution associated to f_1 during dt, hence:

$$OP_{f1}(t+dt) - OP_{f1}(t) = 0$$
$$V_P dt\left[n_S(T_{CZ}) - n_L(T_{HZ})\right] + dz\left[n_{L\phi} - n_{S\phi}\right] = 0$$
$$dz = \frac{dt}{\Delta n_\phi} V_P \, \Delta n_{SL} \quad (3)$$

This relation allows placing the point corresponding to the fringe f_1 at t+dt, at the distance dz of the point corresponding to f_1 at t. This adds an intermediate point to the profile given by $f_1(t)$ and $f_2(t)$. Simultaneously, the same analysis is performed for $f_2(t+dt)$ and fringes of superior orders. An average of 8 to 10 intermediate images is used on a time interval that roughly corresponds to the sliding of 1 fringe.

The data extracted from fringes are then analysed to extract the dendrite profiles in two cutting planes: one along the secondary branches ({100} longitudinal section) and the other between secondary branches ({110} longitudinal section), as depicted in Fig. 2a.

3. Results and discussion

The above analysis was conducted on a selection of dendrites grown with pulling rates ranging from 5 to 20 µm/s.

An example of dendrite profiles in the two cutting planes is given in Fig. 3 for V_P = 20 µm/s. Such profiles are analysed to extract the tip radius. The functions classically used to describe the tip result directly from physical theories of dendritic growth. The easiest method is to follow Ivantsov description and to fit the dendrite shape by a simple parabola. Recent developments integrate the importance of the anisotropy of surface tension and lead to anisotropic shape of the dendrite. Based on the theory of microscopic solvability, Ben Amar and Brener [16] gave a solution for the 3D shape of a dendrite of cubic anisotropy corresponding to a paraboloid corrected by a sum of terms depending on the orientation; the correction terms become more and more important going away from the tip and the parabola approximation can be applied only very close to the tip. Taking into account only the first non-zero correction term

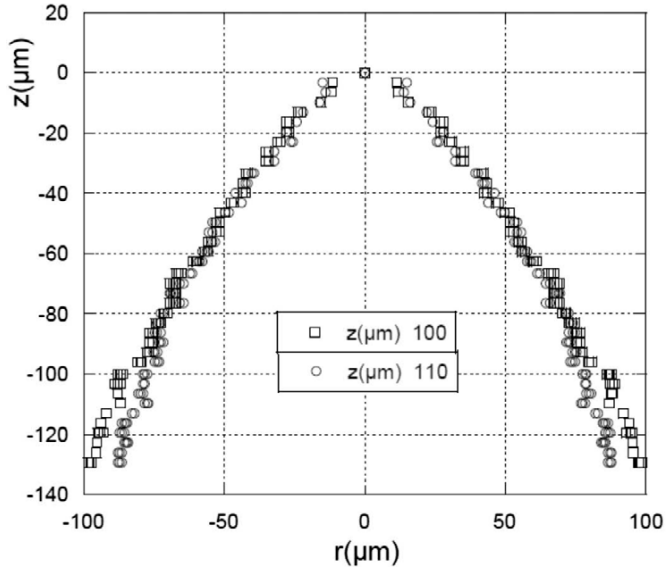

Fig. 3 : Dendrite contours in {100} and {110} planes (Succinonitrile – 0.1 wt% camphor; V_P = 20 µm/s ; G = 17 K/cm)

obtained in case of low anisotropy, this solution can be written in cylindrical polar coordinates (r,ϕ,z):

$$z(r,\phi) = -\frac{r^2}{2R} + A_4 \frac{r^4}{R^3}\cos(4\phi) \quad (4)$$

with A_4, a constant evaluated by the authors at 1/88, independent of anisotropy strength [16].

The correction term of the previous equation grows faster than the leading parabolic term, therefore limiting the validity of this expression quite close from the tip. This led Brener [17] to search for a description valid farther from the tip. In his calculation, the time evolution of the cross-section of the dendrite is studied using the non-axisymmetric shape correction of the tip (eq. 4) as an initial condition. He predicted the development of the 4 dendrite fins so that the contour of the fins is described:

$$\frac{z}{R} = a\left(\frac{x}{R}\right)^{5/3} \quad (5)$$

with x, the interface coordinate normal to the z axis, in a {010} section of the tip (corresponds to a fin) ; and a of the order of unit in case of low anisotropy.

In the following, these different fits are applied to our experimental results.

- ***Parabolic fitting***

Parabolic fits were performed to extract the tip radius. Even if the possible length of fit is low, it appeared that it is sufficient to get two completely independent tip radii depending on the cutting plane, thus underlying the importance of anisotropy. Some trials were carried out to use a smaller fitting length, but the precision is not sufficient to extract correct data in that case as the very extremity of the tip is only very roughly described.

- ***Fitting with parabola corrected by a fourth-order term***

The earlier mentioned dependence of tip radius on the orientation of cutting plane when fitting by parabolas was already pointed out by Lacombe et al. [18] who applied fitting curves including a fourth-order correction (eq. 4) depending on the orientation to get a unique tip radius for all orientations. The same technique was used in our study. The direct determination of A_4 and R simultaneously is impossible in one step since different couples of values are found for the two cutting planes. Therefore, we proceeded by successive steps: by entering the same value of R, the profiles corresponding to the two cutting planes give two different values of A_4 ; the resulting average value of A_4 is used to find new values of R, that are averaged and used to find new values of A_4 and so on until maximum reduction of the differences between the 2 values of both parameters. Results are given in Table 1.

As previously mentioned, the value of A_4 was theoretically evaluated initially at 1/88 = 0.011 [16]. Later, this theoretical approach was slightly modified to integrate anisotropy strength in A_4 which finally led for SCN to a value of ~ 0.006 [19]. Direct experimental measurements for SCN are limited to those of LaCombe et al. [18] who obtained A_4 ~ 0.004 ; this value is also obtained by Karma et al. in

Table 1 : Analysis of dendrite profiles

V_P (μm/s)	Dendrite name	Parabola+4th order correction		Power-law
		R (μm)	A4	β
20	D1	35 ± 2	0.0096 ± 0.0002	1.71 ± 0.02
	D2	35.3 ± 0.9	0.0088 ± 0.0008	1.46 ± 0.03
	D3	33.6 ± 0.4	0.0087 ± 0.0009	1.71 ± 0.04
15	D4	28.0 ± 0.2	0.0057 ± 0.0003	1.60 ± 0.06
	D5	27.1 ± 0.3	0.0049 ± 0.0006	1.56 ± 0.05
10	D6	36.0 ± 0.1	0.0049 ± 0.0004	1.71 ± 0.06
	D7	38.0 ± 0.2	0.0068 ± 0.0003	1.66 ± 0.05
5	D8	28.5 ± 0.3	0.0045 ± 0.0003	1.69 ± 0.08
	D9	27.4 ± 0.4	0.0053 ± 0.0007	1.54 ± 0.09

case of phase-field simulations of 3D dendrites [20]. The order of magnitude experimentally obtained in our work is perfectly consistent with such values but a quite large dispersion is noticeable since values vary from 0.0045 to 0.0096 which roughly corresponds to 0.007 ± 0.002.

The data of table 1 are represented in figure 4 to analyse the effect of pulling rate on tip radius; these data are compared to theoretical radius coming from marginal stability theories [21] and usually verified experimentally in case of diffusive directional growth [4,8] :

$$R = \sqrt{\frac{\Gamma}{\sigma^* \left(m G_C - G \right)}} \qquad (6)$$

with $\sigma^* \sim 0.02$, stability constant

$m = -1.38$ K/wt%, liquidus slope

$\Gamma = 6.49\ 10^{-8}$ Km, Gibbs-Thomson coefficient

G, thermal gradient

G_C, solutal gradient in liquid at the dendrite tip : $G_c = \frac{V_P}{D_L} C_0 (k-1)$

$k \sim 0.2$, partition coefficient

$D_L \sim 0.23\ 10^{-9}$ m^2/s, diffusion coefficient of camphor in liquid SCN

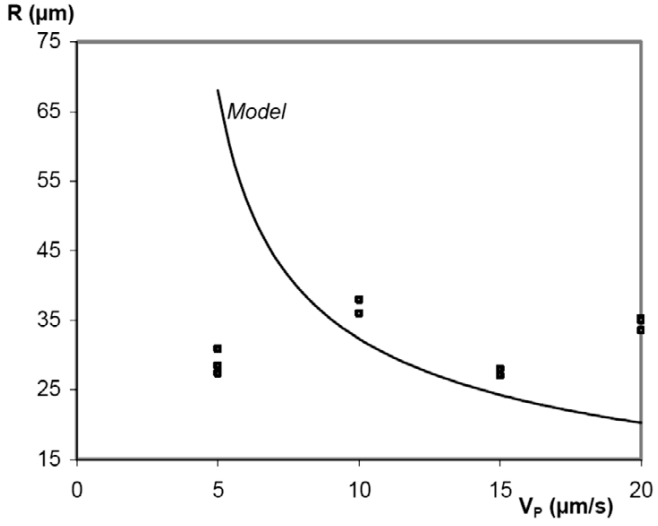

Fig. 4 : Variation of tip radius with pulling rate – Comparison with theory calculated from eq. (6)

The expected decrease of tip radii with growth rate is not verified. The presence of convection in our experiments that strongly modified local parameters of growth is the most likely explanation. Eq. (6) is applied by considering uniform concentration and thermal gradient all along the interface but it has been demonstrated that in our case, where thermal convection is dominant, a very strong radial gradient of concentration exists [22]. Depending on the location on the interface, the local concentration varies on a large scale so that the same tip radius may be obtained for example for a twice lower rate if the local concentration is just locally twice the nominal one. The local thermal gradient G, affecting eq. (6), also varies significantly along the interface. Therefore, valuable comparison with theoretical modeling would require a more systematic characterization of dendrites all along the interface, taking into account local parameters.

- ***Fitting with a power-law***

Lastly, the contour of the dendrite in the {100} plane were fitted with a simple power-law $z = Ax^{\beta}$ and led to the determination of the β exponent. Results are also given in table 1 and can be compared to the theoretical value of eq. (5) equal to 1.67. Our determination led to $\beta = 1.62 \pm 0.08$, which is considered very satisfactory regarding the small fitting length ; this power-law is supposed to better describe areas further away from the tip.

4. Conclusion

This study presents a method based on interferometric analysis to quantitatively characterize the shape of dendrites grown by directional solidification and followed by in situ observation during their whole growth. The specificity of the system is to enable such characterization in case of extended 3D patterns, which has never been reported before. The question of accuracy of measurements and quality of the reconstruction based on interferometric images is discussed through the comparison of the dendrite contours obtained with different geometric modelling of their shapes. A good correlation between experiments and theories is obtained so that characteristic parameters of the fitting laws extracted from our data are consistent with literature. The question of accuracy also stresses the need of new determination of the refractive indices for our materials, in the whole range of their use, as these data are of major importance to get reliable quantitative measurements.

Experiments have been carried out on a device developed in the frame of the DECLIC project (CNES) aiming at the *in situ* and real time observation of directionally grown extended patterns in condition of diffusive transport. This need for experiments in diffusive condition is once more enlightened since strong discrepancies due to convection are here pointed out between our experiments and theoretical analysis built in the limit of diffusive transport. Space experiments planned in 2009-2010 should provide further clarification on the influence of convection on the dendrite shape selection.

Acknowledgements

This study is carried out in the frame of the CNES project of the DECLIC facility for the International Space Station. In particular, the authors are indebted to the support of CNES Toulouse and industrial companies associated to the project.

References

1. Billia B and Fecht H J, in. *A World without Gravity – Research in Space for Health and Industrial Processes*, (eds) Fitton B and Battrick B, ESA SP 1251, European Space Agency, Noordwijk, p. 186 (2001).
2. Huang S C and Glicksman M E, *Acta Metall.,* **29** (1981) 717.
3. Muschol M, Liu D and Cummins H Z, *Phys. Rev. A,* **46** (1992) 1038.
4. Somboonsuk K, Mason J T and Trivedi R, *Met. Trans.,* **15A** (1984) 967.
5. Ivantsov G P, in *Growth of Crystals*, (ed) Shubnikow A.V. and Sheftal N.N. , Consultants Bureau, New-York, **I** (1958) 76
6. Langer J S and Müller-Krumbhaar H, *Acta Metall.,* **26** (1978) 1681.
7. Pomeau Y and Ben Amar M, in *Solids far from equilibrium*, (ed) Godrèche C, Cambridge University Press, Cambridge, (1992) 365
8. Hansen G, Liu S, Lu S Z and Hellawell A, *Journal of Crystal Growth,* **234** (2002) 731.
9. Somboonsuk K and Trivedi R, *Acta Metall.,* **33** (1985) 1051.
10. Bergeon N, Trivedi R, Billia B, Echebarria B, Karma A, Liu S, Weiss C and Mangelinck N, *Adv. in Space Research,* **36** (2005) 80.
11. Noël N, Zamkotsian F, Jamgotchian H and Billia B, *Meas. Sci. Technol.*, **11** (2000) 66.
12. Jamgotchian H, Bergeon N, Benielli D, Voge P and Billia B., *Journal of Microscopy*, **203** (2001) 1.
13. Weiss C, Bergeon N, Mangelinck-Noël N, Billia B, *Material Science Forum,* **508** (2006) 337.
14. Inatomi Y, Miyashita H, Sato E, Kuribayashi K, Itonaga K and Motegi T, *Journal of Crystal Growth,* **130** (1993) 85.
15. MacFarlane R M, Courtens E and Bischofberger T, *Mol. Cryst. Liq. Cryst.,* **35** (1976) 27.
16. Ben Amar M and Brener E, *Phys. Rev. Lett.,* **71** (1993) 589.
17. Brener E, *Phys. Rev. Lett.,* **71** (1993) 3653.
18. LaCombe J C, Koss M B, Fradkov V E and Glicksman M E, *Phys. Rev. E,* **52** (1995) 2778.
19. McFadden G B, Coriell S R and Sekerka R F, *Acta. Mater.,* **48** (2000) 3177.
20. Karma A, Lee Y H and Plapp M., *Phys. Rev. E,* **61** (2000) 3996.
21. Lipton J, Glicksman M E and Kurz W, *Mater. Sci. Eng.,* **65** (1984) 57.
22. Jamgotchian H, Bergeon N, Benielli D, Voge P, Billia B and Guérin R, *Phys. Rev. Lett.,* **87** (2001) 166105.